

This figure "f1.gif" is available in "gif" format from:

<http://arxiv.org/ps/astro-ph/0006010v1>

Turbulent Molecular Cloud Cores: Rotational Properties[†]

Andreas Burkert¹

¹Max-Planck-Institut für Astronomie, Königstuhl 17, D-69117 Heidelberg, Germany;

burkert@mpia-hd.mpg.de

Peter Bodenheimer²

²University of California Observatories/Lick Observatory, Board of Studies in Astronomy and
Astrophysics, University of California, Santa Cruz, CA 95064; peter@ucolick.org

Received _____; accepted _____

ABSTRACT

The rotational properties of numerical models of centrally condensed, turbulent molecular cloud cores with velocity fields that are characterized by Gaussian random fields are investigated. It is shown that the observed line width – size relationship can be reproduced if the velocity power spectrum is a power-law with $P(k) \propto k^n$ and $n = -3$ to -4 . The line-of-sight velocity maps of these cores show velocity gradients that can be interpreted as rotation. For $n = -4$, the deduced values of angular velocity $\Omega = 1.6 \text{ km s}^{-1} \text{ pc}^{-1} \times (R/0.1 \text{ pc})^{-0.5}$ and the scaling relations between Ω and the core radius R are in very good agreement with the observations. As a result of the dominance of long wavelength modes, the cores also have a net specific angular momentum with an average value of $J/M = 7 \times 10^{20} \times (R/0.1 \text{ pc})^{1.5} \text{ cm}^2 \text{ s}^{-1}$ with a large spread. Their internal dimensionless rotational parameter is $\beta \approx 0.03$, independent of the scale radius R . In general, the line-of-sight velocity gradient of an individual turbulent core does not provide a good estimate of its internal specific angular momentum. We find however that the distribution of the specific angular momenta of a large sample of cores which are described by the same power spectrum can be determined very accurately from the distribution of their line-of-sight velocity gradients Ω using the simple formula $j = p\Omega R^2$ where p depends on the density distribution of the core and has to be determined from a Monte-Carlo study. Our results show that for centrally condensed cores the intrinsic angular momentum is overestimated by a factor of 2-3 if $p = 0.4$ is used.

Subject headings: hydrodynamics – stars: formation – ISM: clouds – infrared sources

[†]UCO/Lick Observatory Bulletin, No.....

1. Introduction: Rotating Cloud Cores

Although the rotation in the dense ($n \sim 10^4 - 10^5 \text{ cm}^{-3}$) cores of molecular clouds has small dynamical effects compared with gravity, it has important consequences once a core collapses to form a single star or binary system with associated disks. The distribution of separations of binary systems, the distribution of disk sizes, and the properties of emerging planetary systems all depend on the range of angular momenta among the different cores as well as on the angular momentum distributions within individual cores. Most theoretical calculations of the collapse of rotating cloud cores (see Bodenheimer et al. 2000 for a review) assume as an initial condition that the core is uniformly rotating; furthermore, the observational determination of rotational properties of cores are based upon a model of uniform rotation (Goodman et al. 1993; Goldsmith & Arquilla 1985; Menten et al. 1984.) However the material in molecular clouds is observed to have supersonic line widths over a wide range of scales indicating a supersonic, irregular velocity field. The line width correlates with size, providing evidence that has been interpreted in terms of turbulent motions (Larson 1981, Myers & Gammie 1999; see below), probably associated with a magnetic field (Arons & Max 1975). Observed line profiles in molecular clouds have been shown to be consistent with Gaussian velocity fields with a Kolmogorov spectrum (Dubinski, Narayan, & Phillips 1995, Klessen 2000). Even cores on scales of 0.1 pc or less show non-thermal motions whose velocity dispersion is comparable to, but definitely less than, the sound speed (Barranco & Goodman 1998). Thus the rotational properties of cores may be more complicated than the simple law of uniform rotation would indicate.

The evidence for rotation in the cores of molecular clouds (Myers & Benson 1983; Goldsmith & Arquilla 1985) consists of observations of gradients in the line-of-sight velocity along cuts across the cores. Goodman et al. (1993; updated by Barranco & Goodman 1998) have observed cores in the size range 0.06 to 0.6 pc in the NH_3 molecule, finding evidence of rotation in 29 out of 43 cases studied and finding velocity gradients Ω in the range 0.3 to 3 $\text{km s}^{-1} \text{ pc}^{-1}$ (corresponding to $10^{-14} - 10^{-13} \text{ s}^{-1}$). Over this range of scales, Ω scales roughly as $R^{-0.4}$, and the specific angular momentum $j \equiv J/M$ as inferred from Ω scales roughly as $R^{1.6}$, with a value of $j \approx 10^{21} \text{ cm}^2 \text{ s}^{-1}$ on the smallest scales measured. The dimensionless quantity β , defined as the ratio of rotational kinetic energy divided by the absolute value of the gravitational energy, shows no trend with R and has a mean value of about 0.03 with a large scatter. It is also found that cores tend to have gradients that are not in the same direction as gradients found on larger scales in the immediate surroundings (Barranco & Goodman 1998), an effect which again suggests the presence of turbulence.

In this paper, following previous suggestions (Goldsmith & Arquilla 1985; Goodman et al. 1993;

Dubinski et al. 1995) regarding the connection between turbulence and rotation, we investigate a possible origin of rotation in turbulent cores and investigate the relationship between their line-of-sight velocity maps and their intrinsic rotational properties. Unfortunately, a complete and comprehensive theory of turbulence does still not exist. We therefore adopt the standard simple approach to describe the velocity field inside such cores by a Gaussian random field. This model assumes random phase correlations between the different modes. In order to analyze a large statistical sample we also neglect the coupling between the density and velocity field, which is justified as the flow in observed molecular cloud cores is mildly subsonic. In subsequent papers we plan to include this coupling and to analyze in detail how the rotational properties change during the evolution and collapse of turbulent cores with initial Gaussian random fields.

Here, we try to answer the question whether uniform rotation is a reasonable assumption for such cores, i.e. whether the velocity gradients, determined from line-of-sight velocity maps, in combination with the assumption of rigid body rotation, provide a good estimate of the intrinsic specific angular momenta of turbulent cores. We show that even if the motions in cores are completely random, in many cases systematic velocity gradients in the line-of-sight components of the velocity are present with values that are in good agreement with the observations, that the cores can have net intrinsic angular momenta, and that the line-of-sight velocity gradients provide on average a good estimate of their distribution of specific angular momenta. In §2 we describe how random velocity distributions can be derived that are consistent with observed line width – size relations. §3 outlines how the projected angular velocity Ω is determined from line-of-sight velocity maps. §4 describes the results of a set of 4000 different realizations of the turbulent velocity field and shows that the model can explain the typical values of Ω , j , and β observed in molecular cores. That the model also explains the trends with core size is shown in §5. §6 explores the amount of intrinsic specific angular momentum of turbulent cores and the relationship between the intrinsic angular momentum and the projected velocity gradient. Conclusions are presented in §7.

2. Construction of Models

The velocity field $\vec{v}(\vec{x})$ can be characterized by its Fourier modes

$$\vec{v}(\vec{x}) = \frac{1}{(2\pi)^3} \text{Re} \left[\int \vec{\hat{v}}(\vec{k}) e^{i\vec{k}\vec{x}} d^3k \right] \quad (1)$$

Dubinski et al. (1995) show that line-of sight velocity profiles in molecular clouds are consistent with a

Gaussian random field with a Kolmogorov spectrum $P(k) \propto k^{-11/3}$. The relation between the turbulent spectrum and the line width - size relation has been discussed by Gammie & Ostriker (1996) and Myers & Gammie (1999); the latter authors also suggest random relative phases for the spectral components. Assuming an isotropic velocity field, the Fourier components $\vec{v}(\vec{k})$ are completely specified by the power spectrum $P(k) = \langle \vec{v}^2(k) \rangle$ where $k = |\vec{k}|$. The power spectrum will depend on the physical properties of the velocity field which characterizes molecular clouds and has to be determined from the observations. Larson (1981) showed that the observed internal velocity dispersion σ of a molecular cloud region is well correlated with its length scale λ , following approximately a Kolmogorov law

$$\sigma(\lambda) \sim \lambda^q. \quad (2)$$

with $q \approx 0.38$. Later work found that line width scales with clump size roughly according to $\sigma \sim \lambda^{0.5}$ (Leung, Kutner, & Mead 1982; Scoville, Sanders, & Clemens 1986; Solomon et al. 1987). Additional studies (Fuller & Myers 1992; Caselli & Myers 1995; Myers & Fuller 1992) measured slopes in the range 0.25 to 0.75. In a more recent investigation, Goodman et al. (1998) find that the power-law slope q depends somewhat on λ with virtually constant line widths ($q = 0$) for $\lambda < 0.1$ pc and $q = 0.5$ for larger cores. Given equation (2), the power spectrum must also follow a power-law

$$P(k) \propto k^n, \quad (3)$$

if $q > 0$. Its slope depends on the observed value of q , and the relation between q and n can be determined through filtering the velocity field by passing over it a volume of characteristic size λ and filtering out waves with $k < 1/\lambda$. This leads to a variance

$$\sigma^2(\lambda) = \langle \vec{v}^2(\vec{x}) \rangle_\lambda \sim - \int_{1/\lambda}^{\infty} P(k) k^2 dk \sim \lambda^{-(n+3)} \quad (4)$$

Note that the integral in equation (4) converges only if $n < -3$. Comparing equation (4) with equation (2), we can determine n from the observed line width-size relationship:

$$n = -3 - 2q. \quad (5)$$

Typical molecular cloud cores with $q \approx 0.5$ will be characterized by a power-law index $n \approx -4$ (see

also Myers & Gammie 1999). In the following analysis we will explore the turbulent origin of rotation of molecular cores with a velocity power spectrum $-4 \leq n \leq -3$, which seems to cover most of the observed range. The energy spectrum $E(k)$ which corresponds to a velocity power spectrum $P(k) \propto k^n$ depends on the dimensionality d of the flow and is given by (Myers & Gammie 1999) $E(k) \propto k^{n+d-1}$. With $d = 3$ and $n \approx -4$ the corresponding energy spectrum is $E(k) \propto k^{-2}$.

The velocity field is calculated numerically on a Cartesian 3-dimensional grid with N grid cells in each direction (Cen 1992). Due to the limited resolution we only include modes with $\lambda > 2R/N$. This is no severe restriction if N is large enough ($N \geq 16$) as waves with small wavelengths do not contribute to global rotational properties of the cores, which are preferentially determined by waves of $\lambda \sim R$. The results presented below use $N = 64$ with a cutoff at a wavelength of $\lambda < R/32$. Test calculations with larger $N = 256$ and correspondingly smaller cutoff wavelengths show that $N = 64$ gives adequate resolution. After generating the 3-dimensional velocity field \vec{v} using equation (1) we subtract the center-of-mass velocity. We adopt a coordinate system where (x, z) defines the plane of the sky and the y direction is along the line of sight. Adopting a density distribution $\rho(\vec{x})$, we now can generate two-dimensional maps, with $N \times N$ pixels, of density weighted averaged line-of-sight velocities $V_{LS}(x, z)$ which can be analysed and compared with the spectral line maps of observed molecular cloud cores:

$$V_{LS}(x, z) = \frac{\int \rho(\vec{l}) v_y(\vec{l}) d\vec{l}}{\int \rho(\vec{l}) d\vec{l}} \quad (6)$$

where the integration is done along a given line of sight \vec{l} through the entire cube. Observations indicate that cores are in general centrally condensed with roughly Gaussian density distributions (Ward-Thompson et al. 1994; André et al. 1996; review by Bodenheimer et al. 2000). In the following we will use a spherically symmetric density distribution of the form

$$\rho(r) = \rho_c \times \exp\left(-3 \left(\frac{r}{R_{max}}\right)^2\right). \quad (7)$$

where r is the distance from the center, and R_{max} is the outer radius of the core, at which the density is assumed to be a factor 20 smaller than the central value ρ_c . Additional test calculations with a constant density show that the results do not depend critically on the specific choice of the density distribution. Observed cores are typically analysed within a radius R where the surface density is above half the maximum value. Here we scale all physical quantities to a typical molecular core with a radius $R = 0.1$

pc. For a core with a density distribution given by equation (7), $R \approx 0.5R_{max}$. The data presented by Goodman et al. (1993, their table 1) indicate that these cores have a wide range of masses. A rough average value is $M \approx 5 M_{\odot}$, which we adopt as the typical core mass. Their typical 1-dimensional velocity dispersions are $\sigma_{1d} \approx 0.13 \text{ km s}^{-1}$ (Goodman et al. 1998); σ_{1d} determines the amplitude A of the power spectrum $P(k) = A \times k^n$.

3. Determination of the projected angular velocity and the specific angular momentum

In order to compare our models with observations, we analyze the line-of-sight velocity maps V_{LS} (see eq. [6]) using the least-squares method proposed by Goodman et al. (1993), which minimizes the difference between the observed line-of-sight velocity map and the map expected for a rigidly rotating core. To provide an approximate match to the observations, we include only the inner regions of the cores, where the surface density is above the half-maximum value. In the case of rigid body rotation the line-of-sight velocity is given by

$$V_{LS} = V_0 + \omega_z x - \omega_x z \quad (8)$$

where ω_z and ω_x are the z and x coordinates of the three-dimensional angular velocity vector, and V_0 is the velocity of the center of mass. This equation assumes that the rotation axis goes through the center of the core, which is the origin of the coordinate system. Note that we cannot obtain any information about ω_y from the velocity map. To determine ω_x and ω_z we minimize the error ϵ :

$$\epsilon = \sum_i (V_0 + \omega_z x_i - \omega_x z_i - V_{LS,i})^2 \quad (9)$$

where we sum over all pixels i lying within the inner region defined above. Here x_i and z_i are the x and z coordinates of the i th pixel, and $V_{LS,i}$ is the measured line-of-sight velocity in that pixel. We then solve the following set of equations:

$$\frac{\partial \epsilon}{\partial V_0} = \frac{\partial \epsilon}{\partial \omega_z} = \frac{\partial \epsilon}{\partial \omega_x} = 0. \quad (10)$$

Defining the mean value over the (x, z) plane of a quantity q as $\langle q \rangle = \frac{1}{K \times K} \sum_{i=1}^{K \times K} q_i$, where q_i is its value in the i -th pixel and $K = N/2$, and noting that $\langle x \rangle = \langle z \rangle = \langle xz \rangle = 0$, we find

$$V_0 = \langle V_{LS} \rangle = 0$$

$$\begin{aligned}\omega_x &= -\frac{\langle z \cdot V_{LS} \rangle}{\langle z^2 \rangle} \\ \omega_z &= \frac{\langle x \cdot V_{LS} \rangle}{\langle x^2 \rangle}\end{aligned}\tag{11}$$

It can easily be shown that this solution minimizes the error, namely that the second derivatives are all positive. Given ω_x and ω_z , which again are mean quantities averaged over the $K \times K$ surface, we define the projected $\Omega = (\omega_x^2 + \omega_z^2)^{1/2}$ and we determine the angle of the projected rotation axis which is defined by $\tan \alpha = \omega_z/\omega_x$. As an additional rotational property of the core we determine its total specific angular momentum

$$j = \left(\sum m \vec{v} \times \vec{x} \right) / \sum m,\tag{12}$$

where m is the mass of a cell, and the sum goes over all cells of the three-dimensional grid which are located within the projected half-maximum region which is used to determine the projected Ω .

4. The projected rotational properties of turbulent cores

Although the velocity fields drawn from the same $P(k)$ are statistically equivalent, each realization results from a different set of random numbers and therefore is unique. As a result we expect that the projected and intrinsic rotational properties of the cores may differ significantly from one case to the next and will also change as a function of the index n . Examples are shown in Figure 1, which illustrates 3 different line-of-sight velocity maps for each of the cases $n = -4, -3$, and -2 (from top to bottom). The frames in the first column correspond to an example with relatively high j and high Ω , the second, to low j and high Ω , and the third, to both low j and Ω . One can clearly see that with increasing n the power on small scales increases, leading to more substructure and less systematic motion. In the remainder of the paper, we consider only the values $n = -3, -4$, which correspond to the range of observed q values (eq. [2]) in cores (0 to 0.5, respectively).

The left panels of Figure 1 show examples of a systematic velocity gradient which can easily be interpreted as a rotation. Even for $n = -3$ (second row of Fig. 1) we find cases with relatively well-defined velocity gradients. That there indeed exists a global projected velocity gradient that could be interpreted as rigid body rotation is illustrated in Figure 2, which shows the line-of-sight component of the velocity averaged over slits parallel to the projected rotation axis as a function of distance from the axis for

five cases for $n = -4$, similar to that of the upper left panel of Figure 1. The origin of the velocity gradients are dominant long wavelength modes with small phase shifts with respect to the core center, like $v(x) = v_0 \sin(\pi x/R_{max})$. In the inner regions of the projected velocity maps such a wave would indicate a rigid body rotation with $\Omega \approx \pi v_0/R_{max}$. The dashed lines in Figure 2 show the outer (not observed) parts of the cores where $|v|$ reaches a maximum and decreases again.

The probability for observing a certain value of a velocity gradient can be determined as the frequency with which such values would be found given a large number of projected velocity maps, constructed with different sets of random numbers and projection angles. The left panels in Figure 3 show the distributions of Ω (upper panel), j (middle panel), and β (lower panel), for both $n = -4$ and $n = -3$, for a set of 4000 random realizations in each case. Following Goodman et al. (1993) the parameter β and the specific internal angular momentum j are determined from Ω , adopting rigid body rotation and a constant core density:

$$\begin{aligned} j &= 0.4\Omega R^2 \\ \beta &= \frac{\Omega^2 R^3}{3GM} \end{aligned} \tag{13}$$

Here R is the radius of the inner region. These assumptions are not justified in typical turbulent and centrally condensed cores. Whether j as determined from equation (13) does indeed provide a good estimate for the internal specific angular momentum in turbulent cores will be discussed in greater detail in §6.

For $n = -4$, corresponding to the standard observed line width-size relation, one can see a broad distribution in the values of Ω , with a peak at $1.4 \text{ km s}^{-1} \text{ pc}^{-1}$ and an average dispersion of order $1 \text{ km s}^{-1} \text{ pc}^{-1}$. As expected, the width of the distribution and the value at the peak decrease with increasing n . As shown in the second row of Figure 3, the spread of Ω leads also to a large spread in the j values which are determined from Ω , with j peaking at $1.7 \times 10^{21} \text{ cm}^2 \text{ s}^{-1}$. Finally, in the last row of Figure 3, the apparent distribution of the dimensionless rotation parameter β is shown, derived from Ω , which peaks at $\beta \approx 0.03$. The distributions of these three quantities for the case $n = -3$ (dashed lines in the left panels of Fig. 3) peak at values $1/2 - 2/3$ of those found for the case $n = -4$. Because of the large spread, the average of a large number of observations would be required to determine the average rotational properties of turbulent cores with similar statistical properties. For example, the right-hand panels of Figure 3 show the distribution of mean values of Ω , j and β , with each value being the average over 50 different random

realizations. It shows that from a typical observational sample of 50 cores, the average rotational properties can be determined with an accuracy of order 10%.

In summary, our simulations lead to the following characteristic rotational quantities for turbulent cores with n in the range -3 to -4 : $\Omega \approx 0.5 - 2.0 \text{ km s}^{-1} \text{ pc}^{-1}$, $j \approx 0.5 - 2.5 \times 10^{21} \text{ cm}^2 \text{ s}^{-1}$, and $\beta \approx 0.01 - 0.05$, with a large spread in all quantities. These values are in very good agreement with the observations (Goodman et al., 1993) which for cores with radii of 0.1 pc predict $\Omega \approx 1.3 \text{ km s}^{-1} \text{ pc}^{-1}$, $\beta \approx 0.03$ and $j \approx 1.2 \times 10^{21} \text{ cm}^2 \text{ s}^{-1}$.

5. Scaling Relations

Turbulent cores, where the relevant units are the radius R , mass M , and velocity dispersion σ , have a well-defined relationship between j , Ω , β , and size:

$$\begin{aligned} \Omega &\propto \sigma/R \\ j &\propto \sigma R \\ \beta &\propto (\Omega^2 R^3)/M \propto \sigma^2 R/M. \end{aligned} \tag{14}$$

The first of these relations follows from the method of determining Ω (eq. [11]) and the other two follow from equation (13) with the assumption of uniform rotation. Adopting the standard line width–size relation $\sigma \propto R^{0.5}$, we find $\Omega \propto R^{-0.5}$ and $j \propto R^{1.5}$. The scaling relation for β depends on the gravitational energy of the core, so an additional mass–radius relation is needed. Observations indicate that the velocity dispersion $\sigma^2 \propto M/R$, leading to $M \propto R^2$, and to a β which is independent of radius. A similar derivation of the scaling relations has been presented by Goodman et al. (1993). Using these relations and the values for Ω , j and β as derived for 0.1 pc cores, we now can predict the average values of rotational properties of cores with different sizes. Figure 4 shows that the calculated average rotational core properties as function of radius in the range $-4 \leq n \leq -3$ as well as the predicted spread in β , are in very good agreement with the observational data. In fact, in the size range above 0.1 pc , $n = -4$ agrees much better than $n = -3$, consistent with the line width–size relation.

6. The correlation between projected velocity gradient and specific angular momentum

The previous section showed that a Gaussian random velocity field with a power spectrum that is in agreement with the line width–size relationship is a possible explanation of the rotational properties of molecular cloud cores, as inferred from line-of-sight velocity maps. Using this model, we now investigate the relationship between the observed projected velocity gradient Ω and the intrinsic angular momentum j of the cores.

It is generally assumed that Ω provides a good estimate of j . This would certainly be expected in the case of solid body rotation. There, the main uncertainty is the angle i between the line-of-sight direction and the rotation axis. For random orientations, the average value of $\sin^2 i = 2/3$, and the mean specific angular momentum can be determined accurately for a sample of cores of a given size.

However, if cores are characterized by Gaussian random fields the situation is much more complex and the assumption of rigid body rotation is not valid. Now the line-of-sight velocity field does not provide a good estimate of the amplitudes and phases of the various velocity modes in the perpendicular directions. This is demonstrated in Figure 5, which plots Ω versus j for a large sample of cores, generated with a power-spectrum $P(k) \propto k^{-4}$. Ω does not correlate with j . It might at first seem surprising that cores with small specific angular momentum can show large projected velocity gradients. To illustrate this effect let us consider a very simple velocity field with a dominant long-wavelength mode in the x - and y -direction and with zero phase shift with respect to the center:

$$\vec{v} = v_0 \left(\sin\left(\pi \frac{x}{R_{max}}\right) \vec{e}_y + \eta \sin\left(\pi \frac{y}{R_{max}}\right) \vec{e}_x \right). \quad (15)$$

R_{max} is the radius of the core and \vec{e}_x and \vec{e}_y are the unit vectors in the x and y directions, respectively. The case $\eta = -1$ corresponds to a vortex centered at the origin, while the case $\eta = +1$ places the origin at the “saddle point” between four vortex cells. Suppose that the line-of-sight direction is along the y -axis. As Ω is determined from the velocity field inside a radius $r \leq R_{max}/2$, where $\sin(\pi x/R_{max}) \approx \pi x/R_{max}$, the measured velocity gradient will be $\Omega \approx \pi v_0/R_{max}$, independent of η . The left panel of Figure 6 shows the velocity field in the case of $\eta = -1$. The core clearly contains a net angular momentum j around the z -axis and Ω provides a good estimate of j . However, for $\eta = 1$ (right panel of Fig. 6), the net angular momentum is $j = 0$ whereas the value of Ω has not changed.

In summary, turbulent cores are in general not rigid body rotators. Although they could contain a net

angular momentum, as shown in the previous sections, their complex velocity field makes it impossible to determine the intrinsic angular momentum of a core, given its line-of-sight velocity map. This effect results partly from the fact that compressional velocity components introduce line-of-sight velocity gradients that are not related to rotation.

The situation is however much more promising if one considers the angular momentum distribution of a large sample of cores that are all described by the same power spectrum $P(k)$. As P does not depend on the direction of \vec{k} , a set of maps of the line-of-sight velocity contains much more information regarding the internal kinematical properties of the cores. This is shown in Figure 7 which compares the distribution of specific angular momenta $N(j_{pred})$ as inferred from the line-of-sight velocity gradient Ω (dashed lines) with the intrinsic distribution of specific angular momenta $N(j)$ (solid lines) of cores with exponential (Fig. 7a) or constant (Fig. 7b) density profiles, and with $P(k) \propto k^{-4}$. The values of j_{pred} have been calculated from Ω using the equation $j_{pred} = p\Omega R^2$ with $p = 0.14$ for the exponential density sphere and $p = 0.4$ for the constant density distribution. The intrinsic specific angular momentum j , and from this $N(j)$, is determined using the full information of the 3-dimensional velocity field (eq. [12]), summed over the “observed” inner region. The predicted distribution is in excellent agreement with the real distribution if p is chosen carefully taking into account the underlying density profile. For the constant density case the required value of $p = 0.4$ is actually consistent with the real value of the moment of inertia. In the centrally condensed core, however, a value smaller than the actual moment of inertia ($p = 0.26$) is required to fit the actual j -distribution. The distribution of j_{pred} is slightly wider because this value is determined from random projections. Note that the $\sin i$ -correction is not required in this case.

7. Conclusions

Random Gaussian velocity fields with power spectra $P(k) \propto k^{-3}$ to k^{-4} can reproduce both the observed line width – size relationship and the observed projected rotational properties of molecular cloud cores. They therefore can be used in order to investigate their intrinsic velocity fields in detail or to generate initial conditions for simulations of core collapse and single star or binary formation. We have shown that, due to the dominant large-wavelength modes, these cores contain a non-zero specific angular momentum of order $J/M = 7 \times 10^{20} \times (R/0.1\text{pc})^{1.5} \text{ cm}^2 \text{ s}^{-1}$. As a result of the random nature of the velocity field, cores which are statistically identical, that is which are described by the same power spectrum, show a large spread in their rotational properties, which is in qualitative agreement with the large spread in

observed binary periods (Duquennoy & Mayor 1991). However, the median j for pre-main-sequence and main-sequence binaries is about an order of magnitude less (Simon 1992) than the value we derive for the cores.

The line-of-sight velocity gradient does in general not provide a good estimate of the specific angular momentum of a given core. However, on a statistical basis, the distribution of projected velocity gradients Ω can reproduce very well the distribution of the specific angular momenta j , assuming $j = p\Omega R^2$, where p has to be chosen properly through a Monte Carlo study as presented in this paper. In general, p seems to be smaller than the actual value for the moment of inertia in centrally condensed cores. As a result of this effect, the specific angular momenta of cores are overestimated by roughly a factor of 3 if equation (13) is used.

It is somewhat surprising that the shape of the angular momentum distribution as inferred from the line-of-sight velocity gradients using the simple formula of rigid body rotation is in such a good agreement with that of the intrinsic angular momentum distribution of turbulent cores. One possible explanation might be that the fluctuation spectrum is dominated by the large-scale eddies for the values of n that we consider. The effect of projection would normally result in an expectation value of j_{pred} smaller than the actual j . This effect may be compensated through the effects of compressional modes that would contribute to the measured velocity gradient and could explain the similar shape and width of the two distributions. More detailed analysis is necessary to explain this result and to explain the relationship between the intrinsic moment of inertia and the value of p required to fit the intrinsic angular momentum distribution from the distribution of line-of-sight velocity gradients.

In this paper we assumed that the velocity field is uncorrelated with the spectral line emission and adopted a simple spherically symmetric density profile. In reality the velocity field will affect the density distribution and vice versa. In the case of supersonic turbulence the initially Gaussian velocity field will evolve into a system of shocks. Numerical models (e.g. Mac Low et al. 1998, Ostriker et al. 1999) demonstrate that in this case the initial velocity field does indeed not provide a good estimate of the typical dynamical state of an evolved turbulent cloud. However, for the scales which are investigated in the present paper, cloud regions are mildly subsonic and no strong shocks are expected to form. One therefore might not expect a strong evolution into a dynamical state which is very different with respect to the initial power spectrum.

The interaction and dynamical evolution of the velocity and density field in turbulent cores and its

effect on line-of-sight velocity maps as well as the core collapse and fragmentation will be investigated in detail in subsequent papers.

This work was supported in part through National Science Foundation grant AST-9618548, in part through the Deutsche Forschungsgemeinschaft (DFG), and in part through a special NASA astrophysics theory program which supports a joint Center for Star Formation Studies at NASA/Ames Research Center, UC Berkeley, and UC Santa Cruz. We acknowledge helpful conversations with Richard Klein, Robert Fisher, and Chris McKee at a conference in July, 1999, where we learned of their work on the collapse of turbulent molecular clouds. We also would like to thank L. Blitz, A. Goodman, and P. Myers for interesting discussions and the referee, Ralf Klessen, for many important comments. AB thanks the staff of Lick Observatory for the hospitality during his visits and PB thanks the staff of the Max-Planck-Institut für Astronomie for the hospitality during his visits.

REFERENCES

- André, P., Ward-Thompson, D., & Motte, F. 1996, *A&A*, 314, 625
- Arons, J., & Max, C. E. 1975, *ApJ*, 196, L77
- Barranco, J. A., & Goodman, A. A. 1998, *ApJ*, 504, 207
- Bodenheimer, P., Burkert, A., Klein, R. I., & Boss, A. P. 2000, in *Protostars and Planets IV*, ed. V. Mannings, A.P. Boss, & S.S. Russell (Tucson: Univ. Arizona Press), in press
- Caselli, P., & Myers, P.C. 1995, *ApJ*, 446, 665
- Cen, R. 1992, *ApJS*, 78, 341
- Dubinski, J., Narayan, R., & Phillips, G. 1995, *ApJ*, 448, 226
- Duquennoy, A., & Mayor, M. 1991, *A&A*, 248, 485
- Fuller, G.A., & Myers, P.C. 1992, *ApJ*, 384, 523
- Gammie, C. F., & Ostriker, E. C. 1996, *ApJ*, 466, 814
- Goldsmith, P.F., & Arquilla, R. 1985, in *Protostars and Planets II*, ed. D.C. Black & M.S. Matthews (Tucson: Univ. Arizona Press), 137
- Goodman, A., Benson, P., Fuller, G., & Myers, P. 1993, *ApJ*, 406, 528
- Goodman, A., Barranco, J. A., Wilner, D. J., & Heyer, M. H. 1998, *ApJ*, 504, 223
- Klessen, R.S. 2000, *ApJ*, in press
- Larson, R. B. 1981, *MNRAS*, 194, 809
- Leung, C.M., Kutner, M.L., & Mead, K.N. 1982, *ApJ*, 262, 583
- Mac Low, M.-M., Klessen, R.S., Burkert, A., & Smith, M.D. 1998, *Phys. Rev. Lett.*, 80, 2754
- Menten, K. M., Walmsley, C. M., Krügel, E., & Ungerechts, H. 1984, *A&A*, 137, 108
- Myers, P.C., & Benson, P. 1983, *ApJ*, 266, 309

Myers, P.C., & Fuller, G.A. 1992, ApJ, 396, 631

Myers, P.C., & Gammie, C. F. 1999, ApJ, 522, L141

Ostriker, E.C., Gammie, C. F., & Stone, J.M. 1999, ApJ, 513, 259

Scoville, N.Z., Sanders, D.B., & Clemens, D.P. 1986, ApJ, 310, L77

Simon, M. 1992, in ASP Conf. Ser. 32, Complementary Approaches to Double and Multiple Star Research,
ed. H. A. McAlister & W. I. Hartkopf (San Francisco: ASP), 41

Solomon, P.M., Rivolo, A.R., Barrett, J., & Yahil, A. 1987, ApJ, 319, 730

Ward-Thompson, D., Scott, P.F., Hills, R.E., & André, P. 1994, MNRAS, 268, 276

FIGURE CAPTIONS

Fig. 1.— Maps of the normalized line-of-sight velocity for $n = -4$ (*top row*), $n = -3$ (*center row*), and $n = -2$ (*bottom row*) as determined from eq. (6). In the top row, from left to right, the values of Ω in units of $\text{km s}^{-1} \text{pc}^{-1}$ and the intrinsic specific angular momentum j in units of $10^{21} \text{cm}^2 \text{s}^{-1}$ for cores with radii of 0.1 pc are, respectively, (1.9, 0.9), (0.2, 1.0), and (0.4, 0.6). In the center row, these quantities are (0.7, 0.4), (0.06, 0.5), and (0.26, 0.2). In the bottom row, these quantities are (0.16, 0.1), (0.004, 0.1), and (0.06, 0.06). Blue areas correspond to positive velocities (toward the observer), red corresponds to zero velocity, and yellow corresponds to negative velocity. Each frame shows the inner “observed” region with dimensions one-half those of the full N^3 computational grid.

Fig. 2.— Five randomly chosen examples of simulated cores with large projected velocity gradients with $n = -4$, similar to the upper left panel of Figure 1. The line-of-sight velocity (averaged over a strip parallel to the projected rotation axis with width of $R/32$) is plotted as a function of distance to the projected axis as determined by the least-squares method. The dashed lines indicate unobserved regions.

Fig. 3.— Results of 4000 random realizations of turbulent cores. Histograms for the projected velocity gradient Ω (*top*), the specific angular momentum j as inferred from Ω (*center*) and β (*bottom*) as inferred from Ω (see eq. [13]). In the left panels *solid curves* correspond to a power index $n = -4$ and *dashed curves* correspond to $n = -3$. The right panels compare the histograms for $n = -4$ (*solid curves*) with the residual distribution with each value being the average over 50 different random realizations (*filled areas*).

Fig. 4.— Observed values (Goodman et al. 1993; Barranco & Goodman 1998) of β (*top, crosses*), velocity gradients (*center, triangles*), and specific angular momentum (*bottom, stars*) as a function of the size of the core. *Heavy solid curves*: the trends predicted by the model with $n = -4$. *Heavy dashed curves*: the trends predicted by the model with $n = -3$. *Light solid curves*: the half-maximum points of the calculated distribution for the case $n = -4$. *Light dashed curves*: the half-maximum points of the calculated distribution for the case $n = -3$.

Fig. 5.— The projected Ω values of simulated cores ($n = -4$) are plotted as a function of their internal specific angular momentum $j = J/M$.

Fig. 6.— The velocity field which corresponds to eq. (15) is shown with $\eta = -1$ (*left panel*) and $\eta = +1$ (*right panel*). The size of the vectors is linearly proportional to the absolute value of the velocity.

Fig. 7.— The distribution of specific angular momenta for simulated cores, as inferred from the projected velocity gradient determined from the inner region (*dashed lines*), is compared with the intrinsic distribution of their specific angular momenta, calculated from the 3-dimensional velocity field (*solid lines*). *a*): centrally condensed core. *b*): constant density core.

Turbulent Molecular Cloud Cores: Rotational Properties[†]

Andreas Burkert¹

¹Max-Planck-Institut für Astronomie, Königstuhl 17, D-69117 Heidelberg, Germany;

burkert@mpia-hd.mpg.de

Peter Bodenheimer²

²University of California Observatories/Lick Observatory, Board of Studies in Astronomy and
Astrophysics, University of California, Santa Cruz, CA 95064; peter@ucolick.org

Received _____; accepted _____

ABSTRACT

The rotational properties of numerical models of centrally condensed, turbulent molecular cloud cores with velocity fields that are characterized by Gaussian random fields are investigated. It is shown that the observed line width – size relationship can be reproduced if the velocity power spectrum is a power-law with $P(k) \propto k^n$ and $n = -3$ to -4 . The line-of-sight velocity maps of these cores show velocity gradients that can be interpreted as rotation. For $n = -4$, the deduced values of angular velocity $\Omega = 1.6 \text{ km s}^{-1} \text{ pc}^{-1} \times (R/0.1 \text{ pc})^{-0.5}$ and the scaling relations between Ω and the core radius R are in very good agreement with the observations. As a result of the dominance of long wavelength modes, the cores also have a net specific angular momentum with an average value of $J/M = 7 \times 10^{20} \times (R/0.1 \text{ pc})^{1.5} \text{ cm}^2 \text{ s}^{-1}$ with a large spread. Their internal dimensionless rotational parameter is $\beta \approx 0.03$, independent of the scale radius R . In general, the line-of-sight velocity gradient of an individual turbulent core does not provide a good estimate of its internal specific angular momentum. We find however that the distribution of the specific angular momenta of a large sample of cores which are described by the same power spectrum can be determined very accurately from the distribution of their line-of-sight velocity gradients Ω using the simple formula $j = p\Omega R^2$ where p depends on the density distribution of the core and has to be determined from a Monte-Carlo study. Our results show that for centrally condensed cores the intrinsic angular momentum is overestimated by a factor of 2-3 if $p = 0.4$ is used.

Subject headings: hydrodynamics – stars: formation – ISM: clouds – infrared sources

1. Introduction: Rotating Cloud Cores

Although the rotation in the dense ($n \sim 10^4 - 10^5 \text{ cm}^{-3}$) cores of molecular clouds has small dynamical effects compared with gravity, it has important consequences once a core collapses to form a single star or binary system with associated disks. The distribution of separations of binary systems, the distribution of disk sizes, and the properties of emerging planetary systems all depend on the range of angular momenta among the different cores as well as on the angular momentum distributions within individual cores. Most theoretical calculations of the collapse of rotating cloud cores (see Bodenheimer et al. 2000 for a review) assume as an initial condition that the core is uniformly rotating; furthermore, the observational determination of rotational properties of cores are based upon a model of uniform rotation (Goodman et al. 1993; Goldsmith & Arquilla 1985; Menten et al. 1984.) However the material in molecular clouds is observed to have supersonic line widths over a wide range of scales indicating a supersonic, irregular velocity field. The line width correlates with size, providing evidence that has been interpreted in terms of turbulent motions (Larson 1981, Myers & Gammie 1999; see below), probably associated with a magnetic field (Arons & Max 1975). Observed line profiles in molecular clouds have been shown to be consistent with Gaussian velocity fields with a Kolmogorov spectrum (Dubinski, Narayan, & Phillips 1995, Klessen 2000). Even cores on scales of 0.1 pc or less show non-thermal motions whose velocity dispersion is comparable to, but definitely less than, the sound speed (Barranco & Goodman 1998). Thus the rotational properties of cores may be more complicated than the simple law of uniform rotation would indicate.

The evidence for rotation in the cores of molecular clouds (Myers & Benson 1983; Goldsmith & Arquilla 1985) consists of observations of gradients in the line-of-sight velocity along cuts across the cores. Goodman et al. (1993; updated by Barranco & Goodman 1998) have observed cores in the size range 0.06 to 0.6 pc in the NH_3 molecule, finding evidence of rotation in 29 out of 43 cases studied and finding velocity gradients Ω in the range 0.3 to 3 $\text{km s}^{-1} \text{ pc}^{-1}$ (corresponding to $10^{-14} - 10^{-13} \text{ s}^{-1}$). Over this range of scales, Ω scales roughly as $R^{-0.4}$, and the specific angular momentum $j \equiv J/M$ as inferred from Ω scales roughly as $R^{1.6}$, with a value of $j \approx 10^{21} \text{ cm}^2 \text{ s}^{-1}$ on the smallest scales measured. The dimensionless quantity β , defined as the ratio of rotational kinetic energy divided by the absolute value of the gravitational energy, shows no trend with R and has a mean value of about 0.03 with a large scatter. It is also found that cores tend to have gradients that are not in the same direction as gradients found on larger scales in the immediate surroundings (Barranco & Goodman 1998), an effect which again suggests the presence of turbulence.

In this paper, following previous suggestions (Goldsmith & Arquilla 1985; Goodman et al. 1993;

Dubinski et al. 1995) regarding the connection between turbulence and rotation, we investigate a possible origin of rotation in turbulent cores and investigate the relationship between their line-of-sight velocity maps and their intrinsic rotational properties. Unfortunately, a complete and comprehensive theory of turbulence does still not exist. We therefore adopt the standard simple approach to describe the velocity field inside such cores by a Gaussian random field. This model assumes random phase correlations between the different modes. In order to analyze a large statistical sample we also neglect the coupling between the density and velocity field, which is justified as the flow in observed molecular cloud cores is mildly subsonic. In subsequent papers we plan to include this coupling and to analyze in detail how the rotational properties change during the evolution and collapse of turbulent cores with initial Gaussian random fields.

Here, we try to answer the question whether uniform rotation is a reasonable assumption for such cores, i.e. whether the velocity gradients, determined from line-of-sight velocity maps, in combination with the assumption of rigid body rotation, provide a good estimate of the intrinsic specific angular momenta of turbulent cores. We show that even if the motions in cores are completely random, in many cases systematic velocity gradients in the line-of-sight components of the velocity are present with values that are in good agreement with the observations, that the cores can have net intrinsic angular momenta, and that the line-of-sight velocity gradients provide on average a good estimate of their distribution of specific angular momenta. In §2 we describe how random velocity distributions can be derived that are consistent with observed line width – size relations. §3 outlines how the projected angular velocity Ω is determined from line-of-sight velocity maps. §4 describes the results of a set of 4000 different realizations of the turbulent velocity field and shows that the model can explain the typical values of Ω , j , and β observed in molecular cores. That the model also explains the trends with core size is shown in §5. §6 explores the amount of intrinsic specific angular momentum of turbulent cores and the relationship between the intrinsic angular momentum and the projected velocity gradient. Conclusions are presented in §7.

2. Construction of Models

The velocity field $\vec{v}(\vec{x})$ can be characterized by its Fourier modes

$$\vec{v}(\vec{x}) = \frac{1}{(2\pi)^3} \text{Re} \left[\int \vec{\hat{v}}(\vec{k}) e^{i\vec{k}\vec{x}} d^3k \right] \quad (1)$$

Dubinski et al. (1995) show that line-of sight velocity profiles in molecular clouds are consistent with a

Gaussian random field with a Kolmogorov spectrum $P(k) \propto k^{-11/3}$. The relation between the turbulent spectrum and the line width - size relation has been discussed by Gammie & Ostriker (1996) and Myers & Gammie (1999); the latter authors also suggest random relative phases for the spectral components. Assuming an isotropic velocity field, the Fourier components $\vec{v}(\vec{k})$ are completely specified by the power spectrum $P(k) = \langle \vec{v}^2(k) \rangle$ where $k = |\vec{k}|$. The power spectrum will depend on the physical properties of the velocity field which characterizes molecular clouds and has to be determined from the observations. Larson (1981) showed that the observed internal velocity dispersion σ of a molecular cloud region is well correlated with its length scale λ , following approximately a Kolmogorov law

$$\sigma(\lambda) \sim \lambda^q. \quad (2)$$

with $q \approx 0.38$. Later work found that line width scales with clump size roughly according to $\sigma \sim \lambda^{0.5}$ (Leung, Kutner, & Mead 1982; Scoville, Sanders, & Clemens 1986; Solomon et al. 1987). Additional studies (Fuller & Myers 1992; Caselli & Myers 1995; Myers & Fuller 1992) measured slopes in the range 0.25 to 0.75. In a more recent investigation, Goodman et al. (1998) find that the power-law slope q depends somewhat on λ with virtually constant line widths ($q = 0$) for $\lambda < 0.1$ pc and $q = 0.5$ for larger cores. Given equation (2), the power spectrum must also follow a power-law

$$P(k) \propto k^n, \quad (3)$$

if $q > 0$. Its slope depends on the observed value of q , and the relation between q and n can be determined through filtering the velocity field by passing over it a volume of characteristic size λ and filtering out waves with $k < 1/\lambda$. This leads to a variance

$$\sigma^2(\lambda) = \langle \vec{v}^2(\vec{x}) \rangle_\lambda \sim - \int_{1/\lambda}^{\infty} P(k) k^2 dk \sim \lambda^{-(n+3)} \quad (4)$$

Note that the integral in equation (4) converges only if $n < -3$. Comparing equation (4) with equation (2), we can determine n from the observed line width-size relationship:

$$n = -3 - 2q. \quad (5)$$

Typical molecular cloud cores with $q \approx 0.5$ will be characterized by a power-law index $n \approx -4$ (see

also Myers & Gammie 1999). In the following analysis we will explore the turbulent origin of rotation of molecular cores with a velocity power spectrum $-4 \leq n \leq -3$, which seems to cover most of the observed range. The energy spectrum $E(k)$ which corresponds to a velocity power spectrum $P(k) \propto k^n$ depends on the dimensionality d of the flow and is given by (Myers & Gammie 1999) $E(k) \propto k^{n+d-1}$. With $d = 3$ and $n \approx -4$ the corresponding energy spectrum is $E(k) \propto k^{-2}$.

The velocity field is calculated numerically on a Cartesian 3-dimensional grid with N grid cells in each direction (Cen 1992). Due to the limited resolution we only include modes with $\lambda > 2R/N$. This is no severe restriction if N is large enough ($N \geq 16$) as waves with small wavelengths do not contribute to global rotational properties of the cores, which are preferentially determined by waves of $\lambda \sim R$. The results presented below use $N = 64$ with a cutoff at a wavelength of $\lambda < R/32$. Test calculations with larger $N = 256$ and correspondingly smaller cutoff wavelengths show that $N = 64$ gives adequate resolution. After generating the 3-dimensional velocity field \vec{v} using equation (1) we subtract the center-of-mass velocity. We adopt a coordinate system where (x, z) defines the plane of the sky and the y direction is along the line of sight. Adopting a density distribution $\rho(\vec{x})$, we now can generate two-dimensional maps, with $N \times N$ pixels, of density weighted averaged line-of-sight velocities $V_{LS}(x, z)$ which can be analysed and compared with the spectral line maps of observed molecular cloud cores:

$$V_{LS}(x, z) = \frac{\int \rho(\vec{l}) v_y(\vec{l}) d\vec{l}}{\int \rho(\vec{l}) d\vec{l}} \quad (6)$$

where the integration is done along a given line of sight \vec{l} through the entire cube. Observations indicate that cores are in general centrally condensed with roughly Gaussian density distributions (Ward-Thompson et al. 1994; André et al. 1996; review by Bodenheimer et al. 2000). In the following we will use a spherically symmetric density distribution of the form

$$\rho(r) = \rho_c \times \exp\left(-3 \left(\frac{r}{R_{max}}\right)^2\right). \quad (7)$$

where r is the distance from the center, and R_{max} is the outer radius of the core, at which the density is assumed to be a factor 20 smaller than the central value ρ_c . Additional test calculations with a constant density show that the results do not depend critically on the specific choice of the density distribution. Observed cores are typically analysed within a radius R where the surface density is above half the maximum value. Here we scale all physical quantities to a typical molecular core with a radius $R = 0.1$

pc. For a core with a density distribution given by equation (7), $R \approx 0.5R_{max}$. The data presented by Goodman et al. (1993, their table 1) indicate that these cores have a wide range of masses. A rough average value is $M \approx 5 M_{\odot}$, which we adopt as the typical core mass. Their typical 1-dimensional velocity dispersions are $\sigma_{1d} \approx 0.13 \text{ km s}^{-1}$ (Goodman et al. 1998); σ_{1d} determines the amplitude A of the power spectrum $P(k) = A \times k^n$.

3. Determination of the projected angular velocity and the specific angular momentum

In order to compare our models with observations, we analyze the line-of-sight velocity maps V_{LS} (see eq. [6]) using the least-squares method proposed by Goodman et al. (1993), which minimizes the difference between the observed line-of-sight velocity map and the map expected for a rigidly rotating core. To provide an approximate match to the observations, we include only the inner regions of the cores, where the surface density is above the half-maximum value. In the case of rigid body rotation the line-of-sight velocity is given by

$$V_{LS} = V_0 + \omega_z x - \omega_x z \tag{8}$$

where ω_z and ω_x are the z and x coordinates of the three-dimensional angular velocity vector, and V_0 is the velocity of the center of mass. This equation assumes that the rotation axis goes through the center of the core, which is the origin of the coordinate system. Note that we cannot obtain any information about ω_y from the velocity map. To determine ω_x and ω_z we minimize the error ϵ :

$$\epsilon = \sum_i (V_0 + \omega_z x_i - \omega_x z_i - V_{LS,i})^2 \tag{9}$$

where we sum over all pixels i lying within the inner region defined above. Here x_i and z_i are the x and z coordinates of the i th pixel, and $V_{LS,i}$ is the measured line-of-sight velocity in that pixel. We then solve the following set of equations:

$$\frac{\partial \epsilon}{\partial V_0} = \frac{\partial \epsilon}{\partial \omega_z} = \frac{\partial \epsilon}{\partial \omega_x} = 0. \tag{10}$$

Defining the mean value over the (x, z) plane of a quantity q as $\langle q \rangle = \frac{1}{K \times K} \sum_{i=1}^{K \times K} q_i$, where q_i is its value in the i -th pixel and $K = N/2$, and noting that $\langle x \rangle = \langle z \rangle = \langle xz \rangle = 0$, we find

$$V_0 = \langle V_{LS} \rangle = 0$$

$$\begin{aligned}\omega_x &= -\frac{\langle z \cdot V_{LS} \rangle}{\langle z^2 \rangle} \\ \omega_z &= \frac{\langle x \cdot V_{LS} \rangle}{\langle x^2 \rangle}\end{aligned}\tag{11}$$

It can easily be shown that this solution minimizes the error, namely that the second derivatives are all positive. Given ω_x and ω_z , which again are mean quantities averaged over the $K \times K$ surface, we define the projected $\Omega = (\omega_x^2 + \omega_z^2)^{1/2}$ and we determine the angle of the projected rotation axis which is defined by $\tan \alpha = \omega_z/\omega_x$. As an additional rotational property of the core we determine its total specific angular momentum

$$j = \left(\sum m \vec{v} \times \vec{x} \right) / \sum m,\tag{12}$$

where m is the mass of a cell, and the sum goes over all cells of the three-dimensional grid which are located within the projected half-maximum region which is used to determine the projected Ω .

4. The projected rotational properties of turbulent cores

Although the velocity fields drawn from the same $P(k)$ are statistically equivalent, each realization results from a different set of random numbers and therefore is unique. As a result we expect that the projected and intrinsic rotational properties of the cores may differ significantly from one case to the next and will also change as a function of the index n . Examples are shown in Figure 1, which illustrates 3 different line-of-sight velocity maps for each of the cases $n = -4, -3$, and -2 (from top to bottom). The frames in the first column correspond to an example with relatively high j and high Ω , the second, to low j and high Ω , and the third, to both low j and Ω . One can clearly see that with increasing n the power on small scales increases, leading to more substructure and less systematic motion. In the remainder of the paper, we consider only the values $n = -3, -4$, which correspond to the range of observed q values (eq. [2]) in cores (0 to 0.5, respectively).

The left panels of Figure 1 show examples of a systematic velocity gradient which can easily be interpreted as a rotation. Even for $n = -3$ (second row of Fig. 1) we find cases with relatively well-defined velocity gradients. That there indeed exists a global projected velocity gradient that could be interpreted as rigid body rotation is illustrated in Figure 2, which shows the line-of-sight component of the velocity averaged over slits parallel to the projected rotation axis as a function of distance from the axis for

five cases for $n = -4$, similar to that of the upper left panel of Figure 1. The origin of the velocity gradients are dominant long wavelength modes with small phase shifts with respect to the core center, like $v(x) = v_0 \sin(\pi x/R_{max})$. In the inner regions of the projected velocity maps such a wave would indicate a rigid body rotation with $\Omega \approx \pi v_0/R_{max}$. The dashed lines in Figure 2 show the outer (not observed) parts of the cores where $|v|$ reaches a maximum and decreases again.

The probability for observing a certain value of a velocity gradient can be determined as the frequency with which such values would be found given a large number of projected velocity maps, constructed with different sets of random numbers and projection angles. The left panels in Figure 3 show the distributions of Ω (upper panel), j (middle panel), and β (lower panel), for both $n = -4$ and $n = -3$, for a set of 4000 random realizations in each case. Following Goodman et al. (1993) the parameter β and the specific internal angular momentum j are determined from Ω , adopting rigid body rotation and a constant core density:

$$\begin{aligned} j &= 0.4\Omega R^2 \\ \beta &= \frac{\Omega^2 R^3}{3GM} \end{aligned} \tag{13}$$

Here R is the radius of the inner region. These assumptions are not justified in typical turbulent and centrally condensed cores. Whether j as determined from equation (13) does indeed provide a good estimate for the internal specific angular momentum in turbulent cores will be discussed in greater detail in §6.

For $n = -4$, corresponding to the standard observed line width-size relation, one can see a broad distribution in the values of Ω , with a peak at $1.4 \text{ km s}^{-1} \text{ pc}^{-1}$ and an average dispersion of order $1 \text{ km s}^{-1} \text{ pc}^{-1}$. As expected, the width of the distribution and the value at the peak decrease with increasing n . As shown in the second row of Figure 3, the spread of Ω leads also to a large spread in the j values which are determined from Ω , with j peaking at $1.7 \times 10^{21} \text{ cm}^2 \text{ s}^{-1}$. Finally, in the last row of Figure 3, the apparent distribution of the dimensionless rotation parameter β is shown, derived from Ω , which peaks at $\beta \approx 0.03$. The distributions of these three quantities for the case $n = -3$ (dashed lines in the left panels of Fig. 3) peak at values $1/2 - 2/3$ of those found for the case $n = -4$. Because of the large spread, the average of a large number of observations would be required to determine the average rotational properties of turbulent cores with similar statistical properties. For example, the right-hand panels of Figure 3 show the distribution of mean values of Ω , j and β , with each value being the average over 50 different random

realizations. It shows that from a typical observational sample of 50 cores, the average rotational properties can be determined with an accuracy of order 10%.

In summary, our simulations lead to the following characteristic rotational quantities for turbulent cores with n in the range -3 to -4 : $\Omega \approx 0.5 - 2.0 \text{ km s}^{-1} \text{ pc}^{-1}$, $j \approx 0.5 - 2.5 \times 10^{21} \text{ cm}^2 \text{ s}^{-1}$, and $\beta \approx 0.01 - 0.05$, with a large spread in all quantities. These values are in very good agreement with the observations (Goodman et al., 1993) which for cores with radii of 0.1 pc predict $\Omega \approx 1.3 \text{ km s}^{-1} \text{ pc}^{-1}$, $\beta \approx 0.03$ and $j \approx 1.2 \times 10^{21} \text{ cm}^2 \text{ s}^{-1}$.

5. Scaling Relations

Turbulent cores, where the relevant units are the radius R , mass M , and velocity dispersion σ , have a well-defined relationship between j , Ω , β , and size:

$$\begin{aligned} \Omega &\propto \sigma/R \\ j &\propto \sigma R \\ \beta &\propto (\Omega^2 R^3)/M \propto \sigma^2 R/M. \end{aligned} \tag{14}$$

The first of these relations follows from the method of determining Ω (eq. [11]) and the other two follow from equation (13) with the assumption of uniform rotation. Adopting the standard line width–size relation $\sigma \propto R^{0.5}$, we find $\Omega \propto R^{-0.5}$ and $j \propto R^{1.5}$. The scaling relation for β depends on the gravitational energy of the core, so an additional mass–radius relation is needed. Observations indicate that the velocity dispersion $\sigma^2 \propto M/R$, leading to $M \propto R^2$, and to a β which is independent of radius. A similar derivation of the scaling relations has been presented by Goodman et al. (1993). Using these relations and the values for Ω , j and β as derived for 0.1 pc cores, we now can predict the average values of rotational properties of cores with different sizes. Figure 4 shows that the calculated average rotational core properties as function of radius in the range $-4 \leq n \leq -3$ as well as the predicted spread in β , are in very good agreement with the observational data. In fact, in the size range above 0.1 pc , $n = -4$ agrees much better than $n = -3$, consistent with the line width–size relation.

6. The correlation between projected velocity gradient and specific angular momentum

The previous section showed that a Gaussian random velocity field with a power spectrum that is in agreement with the line width–size relationship is a possible explanation of the rotational properties of molecular cloud cores, as inferred from line-of-sight velocity maps. Using this model, we now investigate the relationship between the observed projected velocity gradient Ω and the intrinsic angular momentum j of the cores.

It is generally assumed that Ω provides a good estimate of j . This would certainly be expected in the case of solid body rotation. There, the main uncertainty is the angle i between the line-of-sight direction and the rotation axis. For random orientations, the average value of $\sin^2 i = 2/3$, and the mean specific angular momentum can be determined accurately for a sample of cores of a given size.

However, if cores are characterized by Gaussian random fields the situation is much more complex and the assumption of rigid body rotation is not valid. Now the line-of-sight velocity field does not provide a good estimate of the amplitudes and phases of the various velocity modes in the perpendicular directions. This is demonstrated in Figure 5, which plots Ω versus j for a large sample of cores, generated with a power-spectrum $P(k) \propto k^{-4}$. Ω does not correlate with j . It might at first seem surprising that cores with small specific angular momentum can show large projected velocity gradients. To illustrate this effect let us consider a very simple velocity field with a dominant long-wavelength mode in the x - and y -direction and with zero phase shift with respect to the center:

$$\vec{v} = v_0 \left(\sin\left(\pi \frac{x}{R_{max}}\right) \vec{e}_y + \eta \sin\left(\pi \frac{y}{R_{max}}\right) \vec{e}_x \right). \quad (15)$$

R_{max} is the radius of the core and \vec{e}_x and \vec{e}_y are the unit vectors in the x and y directions, respectively. The case $\eta = -1$ corresponds to a vortex centered at the origin, while the case $\eta = +1$ places the origin at the “saddle point” between four vortex cells. Suppose that the line-of-sight direction is along the y -axis. As Ω is determined from the velocity field inside a radius $r \leq R_{max}/2$, where $\sin(\pi x/R_{max}) \approx \pi x/R_{max}$, the measured velocity gradient will be $\Omega \approx \pi v_0/R_{max}$, independent of η . The left panel of Figure 6 shows the velocity field in the case of $\eta = -1$. The core clearly contains a net angular momentum j around the z -axis and Ω provides a good estimate of j . However, for $\eta = 1$ (right panel of Fig. 6), the net angular momentum is $j = 0$ whereas the value of Ω has not changed.

In summary, turbulent cores are in general not rigid body rotators. Although they could contain a net

angular momentum, as shown in the previous sections, their complex velocity field makes it impossible to determine the intrinsic angular momentum of a core, given its line-of-sight velocity map. This effect results partly from the fact that compressional velocity components introduce line-of-sight velocity gradients that are not related to rotation.

The situation is however much more promising if one considers the angular momentum distribution of a large sample of cores that are all described by the same power spectrum $P(k)$. As P does not depend on the direction of \vec{k} , a set of maps of the line-of-sight velocity contains much more information regarding the internal kinematical properties of the cores. This is shown in Figure 7 which compares the distribution of specific angular momenta $N(j_{pred})$ as inferred from the line-of-sight velocity gradient Ω (dashed lines) with the intrinsic distribution of specific angular momenta $N(j)$ (solid lines) of cores with exponential (Fig. 7a) or constant (Fig. 7b) density profiles, and with $P(k) \propto k^{-4}$. The values of j_{pred} have been calculated from Ω using the equation $j_{pred} = p\Omega R^2$ with $p = 0.14$ for the exponential density sphere and $p = 0.4$ for the constant density distribution. The intrinsic specific angular momentum j , and from this $N(j)$, is determined using the full information of the 3-dimensional velocity field (eq. [12]), summed over the “observed” inner region. The predicted distribution is in excellent agreement with the real distribution if p is chosen carefully taking into account the underlying density profile. For the constant density case the required value of $p = 0.4$ is actually consistent with the real value of the moment of inertia. In the centrally condensed core, however, a value smaller than the actual moment of inertia ($p = 0.26$) is required to fit the actual j -distribution. The distribution of j_{pred} is slightly wider because this value is determined from random projections. Note that the $\sin i$ -correction is not required in this case.

7. Conclusions

Random Gaussian velocity fields with power spectra $P(k) \propto k^{-3}$ to k^{-4} can reproduce both the observed line width – size relationship and the observed projected rotational properties of molecular cloud cores. They therefore can be used in order to investigate their intrinsic velocity fields in detail or to generate initial conditions for simulations of core collapse and single star or binary formation. We have shown that, due to the dominant large-wavelength modes, these cores contain a non-zero specific angular momentum of order $J/M = 7 \times 10^{20} \times (R/0.1\text{pc})^{1.5} \text{ cm}^2 \text{ s}^{-1}$. As a result of the random nature of the velocity field, cores which are statistically identical, that is which are described by the same power spectrum, show a large spread in their rotational properties, which is in qualitative agreement with the large spread in

observed binary periods (Duquennoy & Mayor 1991). However, the median j for pre-main-sequence and main-sequence binaries is about an order of magnitude less (Simon 1992) than the value we derive for the cores.

The line-of-sight velocity gradient does in general not provide a good estimate of the specific angular momentum of a given core. However, on a statistical basis, the distribution of projected velocity gradients Ω can reproduce very well the distribution of the specific angular momenta j , assuming $j = p\Omega R^2$, where p has to be chosen properly through a Monte Carlo study as presented in this paper. In general, p seems to be smaller than the actual value for the moment of inertia in centrally condensed cores. As a result of this effect, the specific angular momenta of cores are overestimated by roughly a factor of 3 if equation (13) is used.

It is somewhat surprising that the shape of the angular momentum distribution as inferred from the line-of-sight velocity gradients using the simple formula of rigid body rotation is in such a good agreement with that of the intrinsic angular momentum distribution of turbulent cores. One possible explanation might be that the fluctuation spectrum is dominated by the large-scale eddies for the values of n that we consider. The effect of projection would normally result in an expectation value of j_{pred} smaller than the actual j . This effect may be compensated through the effects of compressional modes that would contribute to the measured velocity gradient and could explain the similar shape and width of the two distributions. More detailed analysis is necessary to explain this result and to explain the relationship between the intrinsic moment of inertia and the value of p required to fit the intrinsic angular momentum distribution from the distribution of line-of-sight velocity gradients.

In this paper we assumed that the velocity field is uncorrelated with the spectral line emission and adopted a simple spherically symmetric density profile. In reality the velocity field will affect the density distribution and vice versa. In the case of supersonic turbulence the initially Gaussian velocity field will evolve into a system of shocks. Numerical models (e.g. Mac Low et al. 1998, Ostriker et al. 1999) demonstrate that in this case the initial velocity field does indeed not provide a good estimate of the typical dynamical state of an evolved turbulent cloud. However, for the scales which are investigated in the present paper, cloud regions are mildly subsonic and no strong shocks are expected to form. One therefore might not expect a strong evolution into a dynamical state which is very different with respect to the initial power spectrum.

The interaction and dynamical evolution of the velocity and density field in turbulent cores and its

effect on line-of-sight velocity maps as well as the core collapse and fragmentation will be investigated in detail in subsequent papers.

This work was supported in part through National Science Foundation grant AST-9618548, in part through the Deutsche Forschungsgemeinschaft (DFG), and in part through a special NASA astrophysics theory program which supports a joint Center for Star Formation Studies at NASA/Ames Research Center, UC Berkeley, and UC Santa Cruz. We acknowledge helpful conversations with Richard Klein, Robert Fisher, and Chris McKee at a conference in July, 1999, where we learned of their work on the collapse of turbulent molecular clouds. We also would like to thank L. Blitz, A. Goodman, and P. Myers for interesting discussions and the referee, Ralf Klessen, for many important comments. AB thanks the staff of Lick Observatory for the hospitality during his visits and PB thanks the staff of the Max-Planck-Institut für Astronomie for the hospitality during his visits.

REFERENCES

- André, P., Ward-Thompson, D., & Motte, F. 1996, *A&A*, 314, 625
- Arons, J., & Max, C. E. 1975, *ApJ*, 196, L77
- Barranco, J. A., & Goodman, A. A. 1998, *ApJ*, 504, 207
- Bodenheimer, P., Burkert, A., Klein, R. I., & Boss, A. P. 2000, in *Protostars and Planets IV*, ed. V. Mannings, A.P. Boss, & S.S. Russell (Tucson: Univ. Arizona Press), in press
- Caselli, P., & Myers, P.C. 1995, *ApJ*, 446, 665
- Cen, R. 1992, *ApJS*, 78, 341
- Dubinski, J., Narayan, R., & Phillips, G. 1995, *ApJ*, 448, 226
- Duquennoy, A., & Mayor, M. 1991, *A&A*, 248, 485
- Fuller, G.A., & Myers, P.C. 1992, *ApJ*, 384, 523
- Gammie, C. F., & Ostriker, E. C. 1996, *ApJ*, 466, 814
- Goldsmith, P.F., & Arquilla, R. 1985, in *Protostars and Planets II*, ed. D.C. Black & M.S. Matthews (Tucson: Univ. Arizona Press), 137
- Goodman, A., Benson, P., Fuller, G., & Myers, P. 1993, *ApJ*, 406, 528
- Goodman, A., Barranco, J. A., Wilner, D. J., & Heyer, M. H. 1998, *ApJ*, 504, 223
- Klessen, R.S. 2000, *ApJ*, in press
- Larson, R. B. 1981, *MNRAS*, 194, 809
- Leung, C.M., Kutner, M.L., & Mead, K.N. 1982, *ApJ*, 262, 583
- Mac Low, M.-M., Klessen, R.S., Burkert, A., & Smith, M.D. 1998, *Phys. Rev. Lett.*, 80, 2754
- Menten, K. M., Walmsley, C. M., Krügel, E., & Ungerechts, H. 1984, *A&A*, 137, 108
- Myers, P.C., & Benson, P. 1983, *ApJ*, 266, 309

Myers, P.C., & Fuller, G.A. 1992, ApJ, 396, 631

Myers, P.C., & Gammie, C. F. 1999, ApJ, 522, L141

Ostriker, E.C., Gammie, C. F., & Stone, J.M. 1999, ApJ, 513, 259

Scoville, N.Z., Sanders, D.B., & Clemens, D.P. 1986, ApJ, 310, L77

Simon, M. 1992, in ASP Conf. Ser. 32, Complementary Approaches to Double and Multiple Star Research,
ed. H. A. McAlister & W. I. Hartkopf (San Francisco: ASP), 41

Solomon, P.M., Rivolo, A.R., Barrett, J., & Yahil, A. 1987, ApJ, 319, 730

Ward-Thompson, D., Scott, P.F., Hills, R.E., & André, P. 1994, MNRAS, 268, 276

Fig. 1.— Maps of the normalized line-of-sight velocity for $n = -4$ (*top row*), $n = -3$ (*center row*), and $n = -2$ (*bottom row*) as determined from eq. (6). In the top row, from left to right, the values of Ω in units of $\text{km s}^{-1} \text{pc}^{-1}$ and the intrinsic specific angular momentum j in units of $10^{21} \text{ cm}^2 \text{ s}^{-1}$ for cores with radii of 0.1 pc are, respectively, (1.9, 0.9), (0.2, 1.0), and (0.4, 0.6). In the center row, these quantities are (0.7, 0.4), (0.06, 0.5), and (0.26, 0.2). In the bottom row, these quantities are (0.16, 0.1), (0.004, 0.1), and (0.06, 0.06). Blue areas correspond to positive velocities (toward the observer), red corresponds to zero velocity, and yellow corresponds to negative velocity. Each frame shows the inner “observed” region with dimensions one-half those of the full N^3 computational grid.

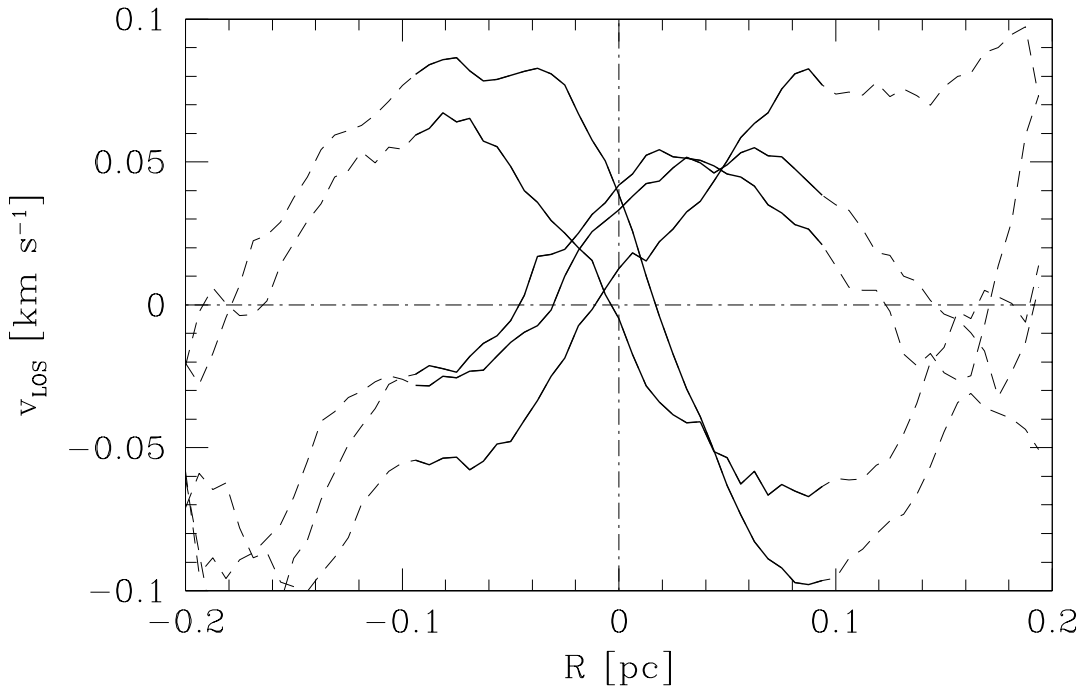


Fig. 2.— Five randomly chosen examples of simulated cores with large projected velocity gradients with $n = -4$, similar to the upper left panel of Figure 1. The line-of-sight velocity (averaged over a strip parallel to the projected rotation axis with width of $R/32$) is plotted as a function of distance to the projected axis as determined by the least-squares method. The dashed lines indicate unobserved regions.

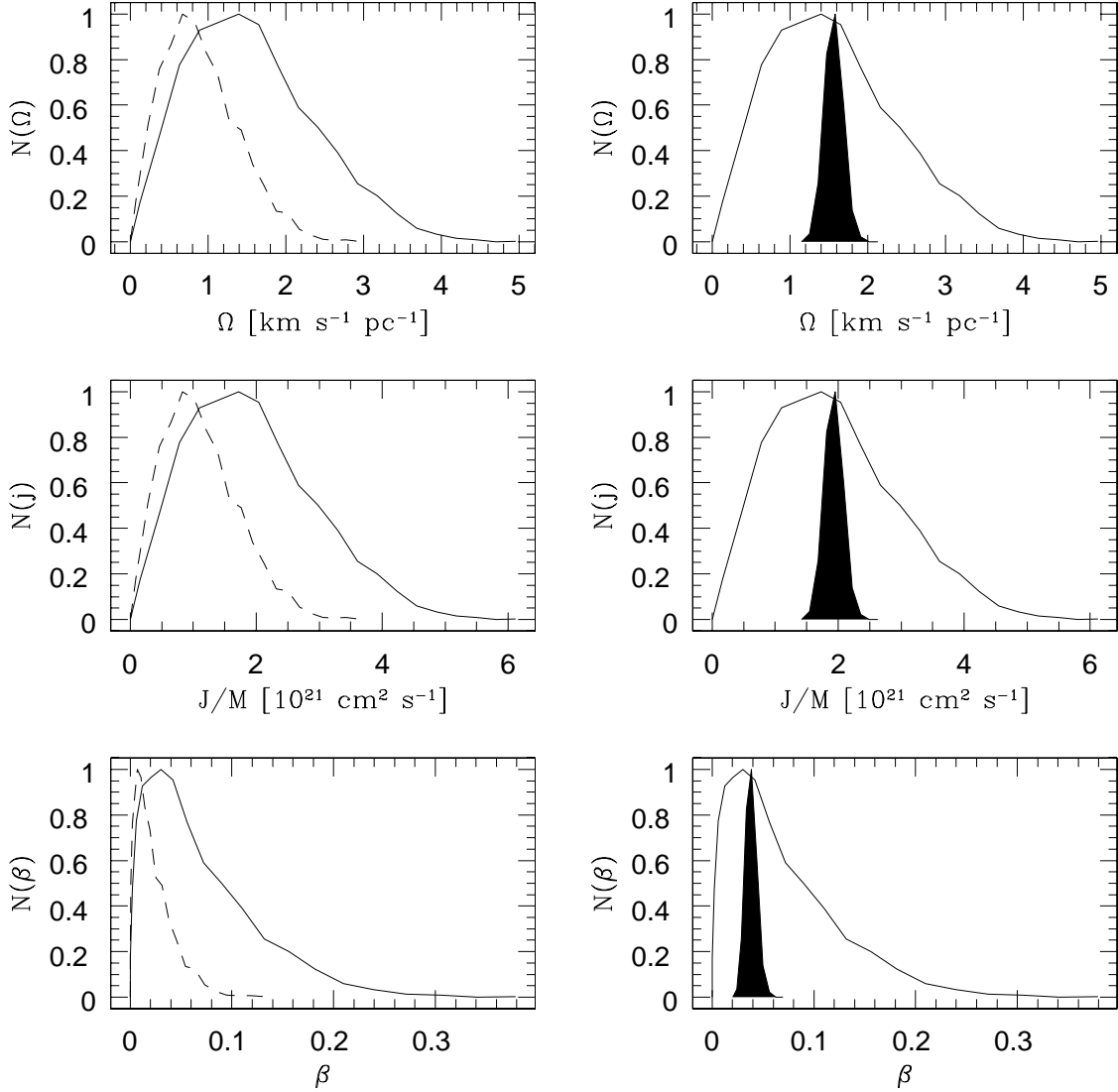


Fig. 3.— Results of 4000 random realizations of turbulent cores. Histograms for the projected velocity gradient Ω (*top*), the specific angular momentum j as inferred from Ω (*center*) and β (*bottom*) as inferred from Ω (see eq. [13]). In the left panels *solid curves* correspond to a power index $n = -4$ and *dashed curves* correspond to $n = -3$. The right panels compare the histograms for $n = -4$ (*solid curves*) with the residual distribution with each value being the average over 50 different random realizations (*filled areas*).

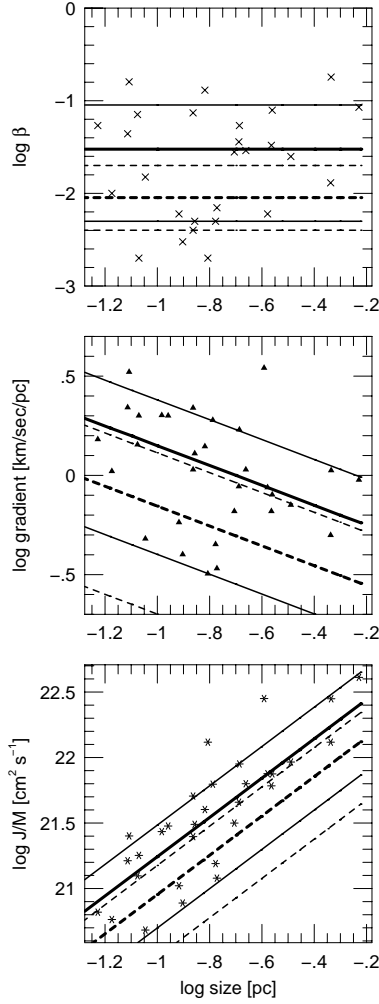


Fig. 4.— Observed values (Goodman et al. 1993; Barranco & Goodman 1998) of β (*top, crosses*), velocity gradients (*center, triangles*), and specific angular momentum (*bottom, stars*) as a function of the size of the core. *Heavy solid curves*: the trends predicted by the model with $n = -4$. *Heavy dashed curves*: the trends predicted by the model with $n = -3$. *Light solid curves*: the half-maximum points of the calculated distribution for the case $n = -4$. *Light dashed curves*: the half-maximum points of the calculated distribution for the case $n = -3$.

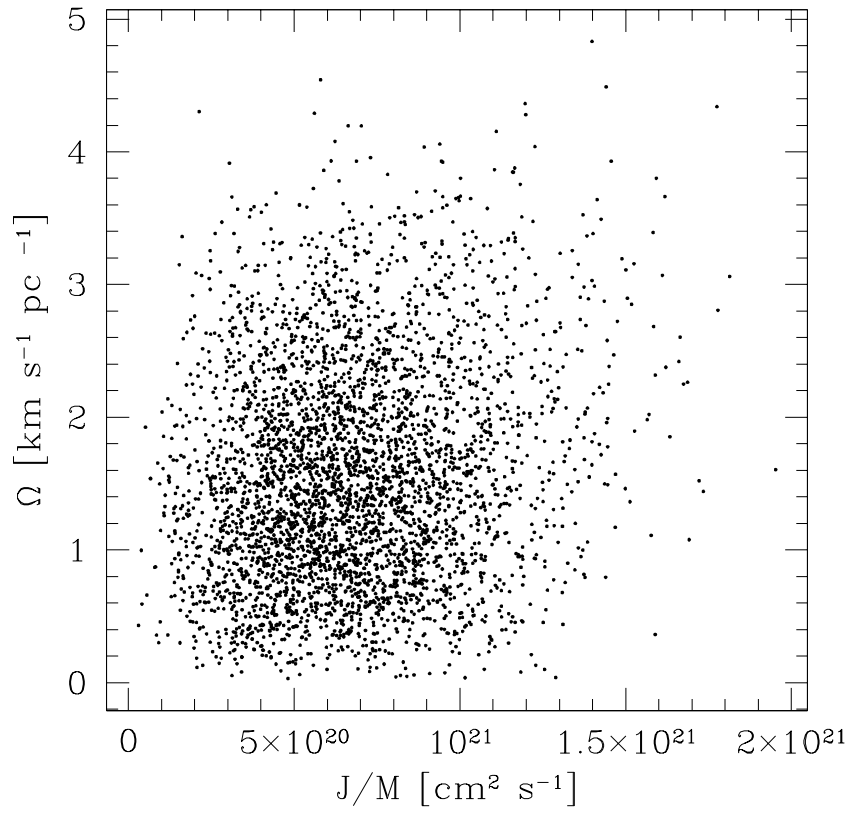


Fig. 5.— The projected Ω values of simulated cores ($n = -4$) are plotted as a function of their internal specific angular momentum $j = J/M$.

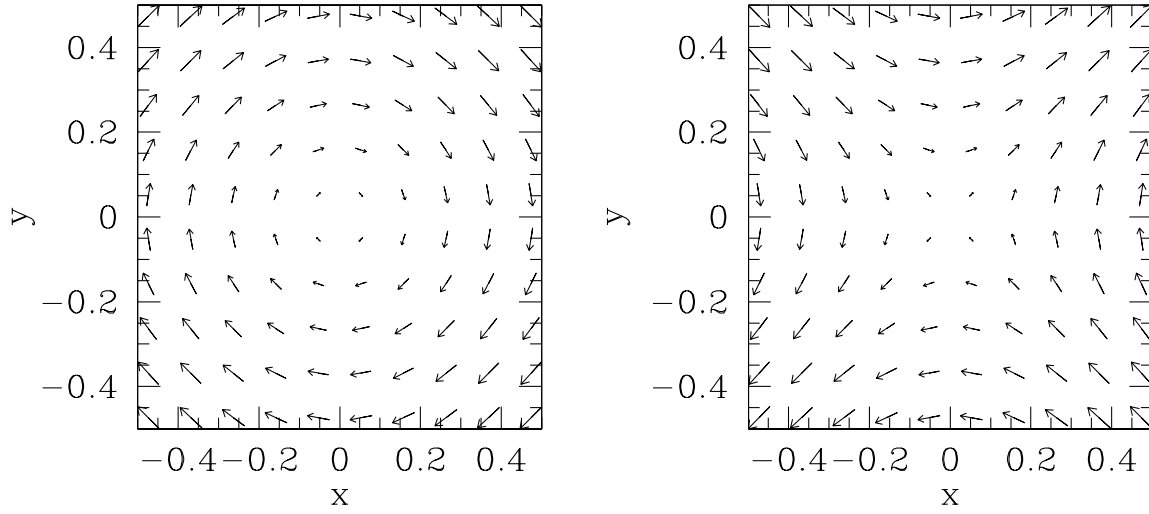


Fig. 6.— The velocity field which corresponds to eq. (15) is shown with $\eta = -1$ (*left panel*) and $\eta = +1$ (*right panel*). The size of the vectors is linearly proportional to the absolute value of the velocity.

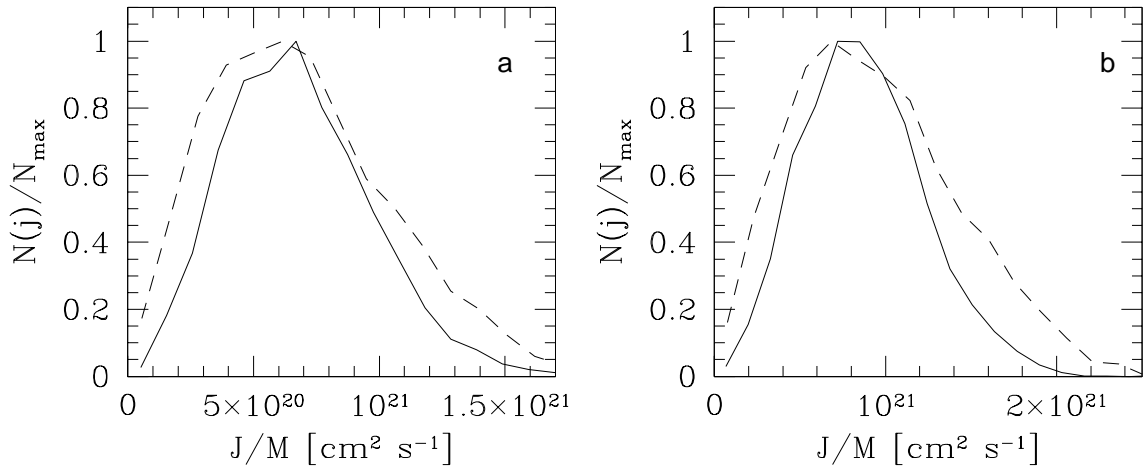


Fig. 7.— The distribution of specific angular momenta for simulated cores, as inferred from the projected velocity gradient determined from the inner region (*dashed lines*), is compared with the intrinsic distribution of their specific angular momenta, calculated from the 3-dimensional velocity field (*solid lines*). *a*): centrally condensed core. *b*): constant density core.